NUCLEAR SCIENCE AND ENGINEERING: **150**, 284–298 (2005)

Generalized Particle Concept for Adjoint Monte Carlo Calculations of Coupled Gamma-Ray–Electron–Positron Transport

N. M. Borisov*

Thomas Jefferson University, Department of Pathology, Anatomy and Cell Biology
1020 Locust Street, Philadelphia, Pennsylvania 19107
and
State Research Center—Institute of Biophysics, 46 Zhivopisnaya St., Moscow, 123182, Russia

and

M. P. Panin

Moscow Engineering Physics Institute (State University)
31 Kashirskoe Shosse, Moscow, 115409, Russia

Received November 20, 2001
Accepted February 28, 2004

Abstract—*Adjoint Monte Carlo methods for coupled transport are developed. The phase-space is extended by the introduction of an additional discrete coordinate (particle type of so-called generalized particle). The generalized particle concept allows the treatment of the transport of mixed radiation as a process with only one particle outgoing from a collision regardless of the physical picture of the interaction. In addition to the forward equation for the generalized particle, the adjoint equation is also derived. The proposed concept is applied to the adjoint equation of the coupled gamma-ray–electron–positron transport. Charged particle transport is considered in continuous slowing down approximation and Molière's theory of multiple scattering, for which special adjoint sampling methods are suggested. A new approach to simulation of fixed-energy secondary radiation is implemented into the generalized particle concept. This approach performs fixed-energy secondary radiation simulation as the local energy estimator through the intermediate state with fixed energy. A comparison of forward and adjoint calculations for energy absorption shows the same results for radionuclide energies with and without electron equilibrium. Adjoint methods show greater efficiency in thin slabs.*

I. INTRODUCTION

The complexity of the description of the coupled particle transport with the linear Pierls equation is connected with generation, at a collision, of secondary particles of various types. As a result, Monte Carlo approaches usually have an analog character and individually simulate every track of secondary particles in one history. According to the authors' point of view, the mentioned complexity can be treated by the generalized consideration of particle collision that interprets changing the outgoing particle type as a transition along an additional phase coordinate.

This generalization is particularly useful for adjoint calculations where there is no apparent physical interpretation of the sampled functions. The relation of adjoint sampling with forward sampling significantly simplifies understanding of the problem and enables numerous methods developed in detail for forward Monte Carlo calculations. Adjoint simulation is known to be more effective in some calculations. It is true, for example, for the highly diffuse in phase-space source and the highly restricted detector (mentioned by Halbleib and Morel[1,2]). Another field where adjoint simulation can give sufficient advantage is connected with importance biasing for the deep penetration problem (see Ref. 3).

*E-mail: nikolay.borisov@jefferson.edu

This paper illustrates the availability of adjoint Monte Carlo simulation of a coupled transport with gamma-ray–electron–positron example.

II. THEORY

II.A. Generalized Transport Approach for Coupled Radiation

Let us examine the coupled transport of particles of different type. To extend the phase-space $\boldsymbol{r}, E, \boldsymbol{\Omega}$, one can introduce an additional discrete coordinate ζ, which runs through integer values from 1 to N, where N is the number of particle types in transport process (photons, electrons, neutrons, etc.). A particle having such coordinates will be called a generalized particle. In the present paper, generalized particles are considered to not interact with each other but only with matter (this interaction has point character), and also only so-called Boltzmann tallies, i.e., tallies that can be derived from the solution to the integral form of the Boltzmann transport equation (when the correlation of the multiple particles outgoing from a collision is not essential for calculations). Non-Boltzmann tallies (such as calculations of pulse-height-spectra or coincident/anticoincident device responses; see more examples in Refs. 4 and 5) are never considered in the present paper. Under such restrictions, the transport equation is linear.

Let $\Sigma_{\nu\zeta}(\boldsymbol{r}, E', \zeta')$ be the cross section of a process happening to a particle with type ζ' and energy E' at a point $\boldsymbol{r}$ and producing ν particles of type ζ. Each of the outgoing particles has emerging energy-angular probability density function (p.d.f.) $f_\zeta(E, \boldsymbol{\Omega})$. Then a differential scattering cross section, which has the meaning of the expected number of particles outgoing from a collision at phase point $\boldsymbol{r}, E, \boldsymbol{\Omega}, \zeta$ will be equal to

$$\Sigma(E', \boldsymbol{\Omega}', \zeta' \rightarrow E, \boldsymbol{\Omega}, \zeta | \boldsymbol{r}) = \sum_{\nu=1}^{\infty} \nu \Sigma_{\nu\zeta}(\boldsymbol{r}, E', \zeta') f_\zeta(E, \boldsymbol{\Omega}) \ . \tag{1}$$

Using the "one-particle" scattering cross section, one can examine the particle balance and write the integro-differential Boltzmann equation of mixed-type particle transport:

$$\begin{aligned} &\boldsymbol{\Omega} \nabla \varphi(\boldsymbol{r}, E, \boldsymbol{\Omega}, \zeta) + \Sigma_t(\boldsymbol{r}, E, \zeta) \varphi(\boldsymbol{r}, E, \boldsymbol{\Omega}, \zeta) \\ &\quad = \sum_{\zeta'=1}^{N} \iint \Sigma(E', \boldsymbol{\Omega}', \zeta' \rightarrow E, \boldsymbol{\Omega}, \zeta | \boldsymbol{r}) \\ &\qquad \times \varphi(\boldsymbol{r}, E', \boldsymbol{\Omega}', \zeta') \, dE' \, d\boldsymbol{\Omega}' + S(\boldsymbol{r}, E, \boldsymbol{\Omega}, \zeta) \ , \end{aligned} \tag{2}$$

where

$\varphi(\boldsymbol{r}, E, \boldsymbol{\Omega}, \zeta)$ = differential flux

$S(\boldsymbol{r}, E, \boldsymbol{\Omega}, \zeta)$ = differential source density.

The adjoint coupled transport equation can be derived from the importance balance:

$$\begin{aligned} &-\boldsymbol{\Omega} \nabla \varphi^+(\boldsymbol{r}, E, \boldsymbol{\Omega}, \zeta) + \Sigma_t(\boldsymbol{r}, E, \zeta) \varphi^+(\boldsymbol{r}, E, \boldsymbol{\Omega}, \zeta) \\ &\quad = \sum_{\zeta'=1}^{N} \iint \Sigma(E, \boldsymbol{\Omega}, \zeta \rightarrow E', \boldsymbol{\Omega}', \zeta' | \boldsymbol{r}) \\ &\qquad \times \varphi^+(\boldsymbol{r}, E', \boldsymbol{\Omega}', \zeta') \, dE' \, d\boldsymbol{\Omega}' \\ &\qquad + D(\boldsymbol{r}, E, \boldsymbol{\Omega}, \zeta) \ , \end{aligned} \tag{3}$$

where $\varphi^+(\boldsymbol{r}, E, \boldsymbol{\Omega}, \zeta)$ is the adjoint flux, or importance of a particle, outgoing from a collision at a point of extended phase-space, i.e., an expected value of detector response from all further random walks of this particle; and $D(\boldsymbol{r}, E, \boldsymbol{\Omega}, \zeta)$ is the detector response function, i.e., a contribution to considered tally per unit path length at phase point $(\boldsymbol{r}, E, \boldsymbol{\Omega}, \zeta)$.

The Monte Carlo method is known to use the integral form of the Boltzmann transport equation rather than the integrodifferential form. It is also more convenient[6] to solve them for forward and adjoint collision densities rather than fluxlike functions φ and φ^+. One can introduce (similar to Refs. 3 and 6) the following: $\psi(\boldsymbol{r}, E, \boldsymbol{\Omega}, \zeta) = \varphi(\boldsymbol{r}, E, \boldsymbol{\Omega}, \zeta) \Sigma_t(\boldsymbol{r}, E, \zeta)$ is the forward incoming collision density; $\chi(\boldsymbol{r}, E, \boldsymbol{\Omega}, \zeta)$ is the forward outgoing collision density; $\chi^+(\boldsymbol{r}, E, \boldsymbol{\Omega}, \zeta) = \varphi^+(\boldsymbol{r}, E, -\boldsymbol{\Omega}, \zeta)$ $\Sigma_t(\boldsymbol{r}, E, \zeta)$ is the adjoint incoming collision density, $\psi^+(\boldsymbol{r}, E, \boldsymbol{\Omega}, \zeta)$ is the adjoint outgoing collision density. It leads to the following integral transport equations for forward and adjoint collision densities:

$$\begin{cases} \psi(\boldsymbol{r}, E, \boldsymbol{\Omega}, \zeta) = \displaystyle\int T(\boldsymbol{r}' \rightarrow \boldsymbol{r} | E, \boldsymbol{\Omega}, \zeta) \chi(\boldsymbol{r}', E, \boldsymbol{\Omega}, \zeta) \, d\boldsymbol{r}' \\ \chi(\boldsymbol{r}, E, \boldsymbol{\Omega}, \zeta) = \displaystyle\sum_{\zeta'=1}^{N} \iint C(E', \boldsymbol{\Omega}', \zeta' \rightarrow E, \boldsymbol{\Omega}, \zeta | \boldsymbol{r}) \\ \qquad \times \psi(\boldsymbol{r}, E', \boldsymbol{\Omega}', \zeta') \, dE' \, d\boldsymbol{\Omega}' \\ \qquad + S(\boldsymbol{r}, E, \boldsymbol{\Omega}, \zeta), \end{cases} \tag{4}$$

$$\begin{cases} \chi^+(\boldsymbol{r}, E, \boldsymbol{\Omega}, \zeta) = \displaystyle\int T(\boldsymbol{r}' \rightarrow \boldsymbol{r} | E, \boldsymbol{\Omega}, \zeta) \psi^+(\boldsymbol{r}', E, \boldsymbol{\Omega}, \zeta) \, d\boldsymbol{r}' \\ \psi^+(\boldsymbol{r}, E, \boldsymbol{\Omega}, \zeta) = \displaystyle\sum_{\zeta'=1}^{N} \iint C^+(E', \boldsymbol{\Omega}', \zeta' \rightarrow E, \boldsymbol{\Omega}, \zeta | \boldsymbol{r}) \\ \qquad \times \chi^+(\boldsymbol{r}, E', \boldsymbol{\Omega}', \zeta') \, dE' \, d\boldsymbol{\Omega}' \\ \qquad + D(\boldsymbol{r}, E, -\boldsymbol{\Omega}, \zeta). \end{cases} \tag{5}$$

where

$$T(\boldsymbol{r}' \rightarrow \boldsymbol{r} | E, \boldsymbol{\Omega}, \zeta) = \frac{\Sigma_t(\boldsymbol{r}, E, \zeta) \exp(-\tau(\boldsymbol{r}' \rightarrow \boldsymbol{r} | E, \zeta)) \delta\left(\boldsymbol{\Omega} - \dfrac{\boldsymbol{r} - \boldsymbol{r}'}{|\boldsymbol{r} - \boldsymbol{r}'|}\right)}{|\boldsymbol{r} - \boldsymbol{r}'|^2} \tag{6}$$

is the transport kernel, τ is the optical distance from $\boldsymbol{r}'$ to $\boldsymbol{r}$ for a ζ-particle of energy E,

$$C(E',\boldsymbol{\Omega}',\zeta' \rightarrow E,\boldsymbol{\Omega},\zeta|\boldsymbol{r}) = \frac{\Sigma(E',\boldsymbol{\Omega}',\zeta' \rightarrow E,\boldsymbol{\Omega},\zeta|\boldsymbol{r})}{\Sigma_t(\boldsymbol{r},E',\zeta')} \quad (7)$$

is the forward collision kernel, and

$$C^+(E',\boldsymbol{\Omega}',\zeta' \rightarrow E,\boldsymbol{\Omega},\zeta|\boldsymbol{r}) = \frac{\Sigma(E,-\boldsymbol{\Omega},\zeta \rightarrow E',-\boldsymbol{\Omega}',\zeta'|\boldsymbol{r})}{\Sigma_t(\boldsymbol{r},E',\zeta')} \quad (8)$$

is the adjoint collision kernel. Note that it is not the system [Eq. (5)] for adjoint collision density-like functions ψ^+ and χ^+, but the system for incoming $\psi^*(\boldsymbol{r},E,\boldsymbol{\Omega},\zeta) = \psi^+(\boldsymbol{r},E,-\boldsymbol{\Omega},\zeta)/\Sigma_t(\boldsymbol{r},E,\zeta)$ and outgoing $\chi^*(\boldsymbol{r},E,\boldsymbol{\Omega},\zeta) = \chi^+(\boldsymbol{r},E,-\boldsymbol{\Omega},\zeta)/\Sigma_t(\boldsymbol{r},E,\zeta) = \varphi^+(\boldsymbol{r},E,\boldsymbol{\Omega},\zeta)$ collision importance, which is really adjoint to the forward integral equation system [Eq. (4)] because in the system for "asterisked" rather than "crossed" functions, input and output arguments are reciprocally transposed as far as it was mentioned by Irving.[6]

Despite the presence of physical collisions with more than one outgoing particle, the forward integral Eq. (4), which describes the coupled transport, uses the phase state of only one generalized particle. It means that we can consider in C-kernel simulation only one outgoing particle (but maybe not of the same type as for the incoming particle). Contrary to the majority of existing Monte Carlo methods for coupled transport, which simulate two or more trajectories of each particle outgoing from a collision, the generalized particle concept assumes sampling only one trajectory without splitting in the simulation algorithm. Because of this biasing, one must perform statistical weight correction by multiplying the particle weight by the result of summing and integrating the collision kernel through all the outgoing coordinates. This weight correction factor for forward simulation is equal to

$$\sum_{\zeta'=1}^{N} \iint C(E,\boldsymbol{\Omega},\zeta \rightarrow E',\boldsymbol{\Omega}',\zeta'|\boldsymbol{r})\,\mathrm{d}E'\,\mathrm{d}\boldsymbol{\Omega}' = \frac{\sum_{m=1}^{\infty} m\Sigma_m(\boldsymbol{r},E,\zeta)}{\Sigma_t(\boldsymbol{r},E,\zeta)}\ , \quad (9)$$

where Σ_m is the cross section of a process with m outgoing particles regardless of their type. As one can see, for forward simulation this factor is the expected number of particles outgoing from a collision. The scheme of forward and adjoint simulation is presented in Fig. 1. Forward random histories begin in source S; adjoint random histories begin in detector D. Lines with arrows represent realized random particle trajectories; lines without arrows represent those not realized during the random game. For expected value conservation, statistical weight W_i should be corrected at every collision.

II.B. Fixed Energy State as Generalized Particle

Simulation of fixed-energy secondary radiation (annihilation photons, characteristic X-rays, Auger electrons, etc.) is one of the most complicated points of adjoint Monte Carlo methods. These difficulties are caused by zero probability of reaching the fixed value from continuous distribution, which was mentioned quite early (however, without a proposed solution), e.g., by Kalos.[7] Later, Halbleib[2] proposed only a restricted method for these problems. Recently, Hoogenboom[8] considered only neutral particles in the transport process. Here, the possible approach to the problem without any evident restrictions (for Boltzmann tallies) is presented.

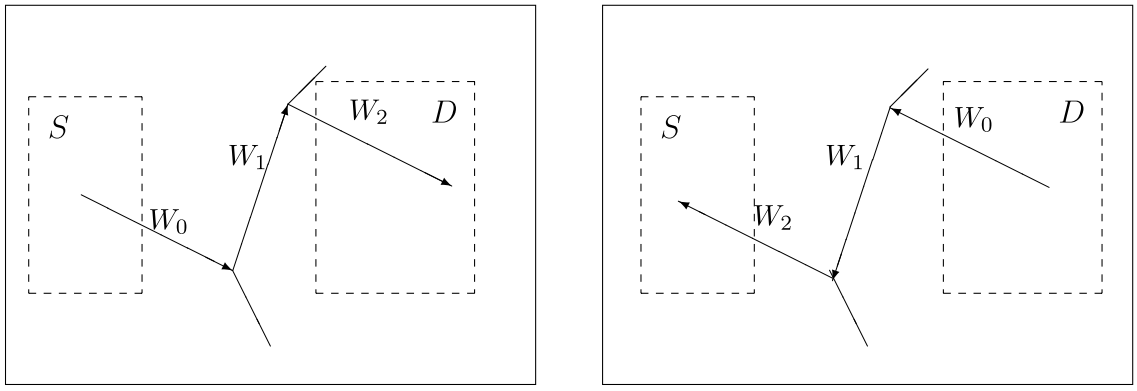

Fig. 1. Application of generalized particle concept to (a) forward and (b) adjoint Monte Carlo simulation.

The generation of secondary fixed energy radiation can be described by the introduction of a singular member to the generalized particle cross section. This part uses the Dirac $\delta(\ldots)$ function in energy and Kronecker symbol $\delta_{\zeta X}$:

$$\Sigma_{sing}(E', \mathbf{\Omega}', \zeta' \rightarrow E, \mathbf{\Omega}, \zeta | \boldsymbol{r}) = \nu \Sigma_X(\boldsymbol{r}, E', \zeta') \delta(E - E_X) f_X(\mathbf{\Omega}' \rightarrow \mathbf{\Omega}) \delta_{\zeta X} \ ,$$

where

Σ_X = cross section of generation process

ν = number of particles of type X with fixed-energy E_X outgoing from a collision.

Now we examine the probabilities for "regular-singular" and "regular-regular" adjoint transitions. Because of the mentioned singularity, these probabilities do not have the same dimension:

$$P^+_{reg \rightarrow sing}(\boldsymbol{r}') = \frac{\Sigma_{reg}(E_X, X \rightarrow E', \zeta' | \boldsymbol{r}')}{\Sigma_t(\boldsymbol{r}', E', \zeta')}$$

and

$$P^+_{reg \rightarrow reg}(\boldsymbol{r}') = \sum_{\zeta=1}^{N} \int \frac{\Sigma(E, \zeta \rightarrow E', \zeta' | \boldsymbol{r}') \, \mathrm{d}E}{\Sigma_t(\boldsymbol{r}', E', \zeta')} \ .$$

However, the subsequent "singular-regular" transition is described by the kernel, whose integral through all the outgoing coordinates is

$$P^+_{sing \rightarrow reg}(\boldsymbol{r}) = \nu \sum_{\zeta=1}^{N} \int \frac{\Sigma_X(\boldsymbol{r}, E, \zeta) \, \mathrm{d}E}{\Sigma_t(\boldsymbol{r}, E_X, X)} \ .$$

The product of $P^+_{reg \rightarrow sing} \times P^+_{sing \rightarrow reg}$ has unitary dimension and may be compared with $P^+_{reg \rightarrow reg}$.

According to these considerations, one can formulate an approach to the simulation of adjoint fixed-energy radiation for adjoint particle, entering a collision in regular state $\boldsymbol{r}', E', \mathbf{\Omega}', \zeta'$.

Step 1: With the probability $P^+_{reg \rightarrow sing} P^+_{sing \rightarrow reg} / (P^+_{reg \rightarrow sing} P^+_{sing \rightarrow reg} + P^+_{reg \rightarrow reg})$ play transition to the singular state, set $E = E_X$, $\zeta = X$, and choose $\mathbf{\Omega}_X$ from the distribution $f_{scat}(\mathbf{\Omega}' \rightarrow \mathbf{\Omega}_X) = \Sigma_{reg}(E_X, -\mathbf{\Omega}_X, X \rightarrow E', -\mathbf{\Omega}', \zeta' | \boldsymbol{r}') / \Sigma_{reg}(E_X, X \rightarrow E', \zeta' | \boldsymbol{r}')$. With the probability $P^+_{reg \rightarrow reg} / (P^+_{reg \rightarrow sing} P^+_{sing \rightarrow reg} + P^+_{reg \rightarrow reg})$ play the transition to the regular state $\boldsymbol{r}', E, \mathbf{\Omega}, \zeta$ according to the regular part of the adjoint collision kernel.

Step 2: If a regular interaction channel was chosen, multiply the statistical weight of the particle by the ratio of unbiased f_{reg} and biased simulated g_{reg} regular-regular transitional functions, which are equal to

$$W_{reg} = \frac{f_{reg}(E', \mathbf{\Omega}', \zeta' \rightarrow E, \mathbf{\Omega}, \zeta | \boldsymbol{r}')}{g_{reg}(E', \mathbf{\Omega}', \zeta' \rightarrow E, \mathbf{\Omega}, \zeta | \boldsymbol{r}')} = \frac{C^+(E', \mathbf{\Omega}', \zeta' \rightarrow E, \mathbf{\Omega}, \zeta | \boldsymbol{r}')}{\dfrac{P^+_{reg \rightarrow reg}(\boldsymbol{r}')}{P^+_{reg \rightarrow sing}(\boldsymbol{r}') P^+_{sing \rightarrow reg}(\boldsymbol{r}') + P^+_{reg \rightarrow reg}(\boldsymbol{r}')} \dfrac{C^+(E', \mathbf{\Omega}', \zeta' \rightarrow E, \mathbf{\Omega}, \zeta | \boldsymbol{r}')}{P^+_{reg \rightarrow reg}(\boldsymbol{r}')}}$$

$$= P^+_{reg \rightarrow sing}(\boldsymbol{r}') P^+_{sing \rightarrow reg}(\boldsymbol{r}') + P^+_{reg \rightarrow reg}(\boldsymbol{r}') \ .$$

Step 3: Simulate the transport kernel T to move the particle from the point $\boldsymbol{r}'$ to the point $\boldsymbol{r}$.

Step 4: If on step 1 a regular channel was chosen, just return to step 1 again. Otherwise, simulate the transition to regular state proportionally to function $C^+_{sing \rightarrow reg}(E_X, \mathbf{\Omega}_X, X \rightarrow E, \mathbf{\Omega}, \zeta | \boldsymbol{r}) = \nu f_X(-\mathbf{\Omega} \rightarrow -\mathbf{\Omega}_X) \Sigma_X(\boldsymbol{r}, E, \zeta) / \Sigma_t(\boldsymbol{r}, E_X, X)$.

Step 5: If on step 1 a singular channel was chosen, multiply the statistical weight of the particle by a correction factor that is equal to the ratio of unbiased f_{sing} and biased simulated g_{sing} regular-singular-regular transitional functions:

$$W_{sing} = \frac{f_{sing}(E', \mathbf{\Omega}', \zeta' \rightarrow E, \mathbf{\Omega}, \zeta | \boldsymbol{r}')}{g_{sing}(E', \mathbf{\Omega}', \zeta' \rightarrow E, \mathbf{\Omega}, \zeta | \boldsymbol{r}')}$$

$$= \frac{\dfrac{\Sigma(E_X, -\mathbf{\Omega}_X, X \rightarrow E', -\mathbf{\Omega}', \zeta | \boldsymbol{r})}{\Sigma_t(\boldsymbol{r}', E', \zeta')} T(\boldsymbol{r}' \rightarrow \boldsymbol{r} | E_X, X) \dfrac{\nu \Sigma_X(\boldsymbol{r}, E, \zeta) f_X(-\mathbf{\Omega} \rightarrow -\mathbf{\Omega}_X)}{\Sigma_t(\boldsymbol{r}, E_X, X)}}{\dfrac{P^+_{reg \rightarrow sing}(\boldsymbol{r}') P^+_{sing \rightarrow reg}(\boldsymbol{r}')}{P^+_{reg \rightarrow sing}(\boldsymbol{r}') P^+_{sing \rightarrow reg}(\boldsymbol{r}') + P^+_{reg \rightarrow reg}(\boldsymbol{r}')} f_{scat}(\mathbf{\Omega}' \rightarrow \mathbf{\Omega}_X) T(\boldsymbol{r}' \rightarrow \boldsymbol{r} | E_X, X) \dfrac{\Sigma_X(\boldsymbol{r}, E, \zeta) f_X(-\mathbf{\Omega} \rightarrow -\mathbf{\Omega}_X)}{\displaystyle\sum_{\zeta=1}^{\infty} \int \Sigma_X(\mathbf{r}, E, \zeta) \, \mathrm{d}E}} \ .$$

According to the definitions previously given, one can obtain after eliminating the equal factors below and above the fraction line that

$$W_{sing} = \left(P^{+}_{reg\to sing}(\boldsymbol{r}\,')P^{+}_{sing\to reg}(\boldsymbol{r}\,') + P^{+}_{reg\to reg}(\boldsymbol{r}\,')\right)\frac{P^{+}_{sing\to reg}(\boldsymbol{r})}{P^{+}_{sing\to reg}(\boldsymbol{r}\,')} \quad .$$

Then return to step 3.

If in some processes secondary radiation with more than one possible fixed energy (e.g., E_1, E_2, etc.) can appear, then for each of the fixed-energy states E_i, the values $P^{+}_{reg\to sing_i}$ and $P^{+}_{sing_i\to reg}$ should be calculated and their products should be compared with each other as well as with $P^{+}_{reg\to reg}$ to choose the proper interaction channel in the random walk game.

The presence of a fixed-energy state in the transport model adds the extra part with the delta-function to the detector function: $D(\boldsymbol{r},E,\boldsymbol{\Omega},\zeta)\delta(E-E_X)\delta_{\zeta X}$. To treat random histories starting from continuous and discrete energies independently, using separate normalization for continuous and discrete cases, which have different dimensions,

$$W_0^{reg} = \sum_{\zeta=1}^{N}\iiint D(\boldsymbol{r},E,\boldsymbol{\Omega},\zeta)\,\mathrm{d}\boldsymbol{r}\,\mathrm{d}E\,\mathrm{d}\boldsymbol{\Omega}$$

and

$$W_0^{sing} = \iint D(\boldsymbol{r},E_X,\boldsymbol{\Omega},X)\,\mathrm{d}\boldsymbol{r}\,\mathrm{d}\boldsymbol{\Omega} \quad ,$$

respectively, one has to multiply the statistical weight for the history started from the singular state when simulating the transition from singular to regular state according to function $\nu\Sigma_X(\boldsymbol{r},E,\zeta)/\Sigma_t(\boldsymbol{r},E_X,X)$, by the integral $P^{+}_{sing\to reg}$ from this transition function.

III. FORWARD COUPLED PHOTON-ELECTRON-POSITRON TRANSPORT SAMPLING IN CONTINUOUS SLOWING DOWN APPROXIMATION

The problem of absorbed energy spatial distribution in thin layers from the primary gamma-ray source (which is important, e.g., for response calculations in thermoluminescent dosimeters), was chosen as an example of the application described in Sec. II concepts. In thin slabs, where electron equilibrium does not exist, the account of electrons and positrons is essential. From here on, coupled transport of three types of particles—photons (symbolically $\zeta=\gamma$), electrons ($\zeta=e$), and positrons ($\zeta=e^{+}$)—is considered. For photons, three interaction processes were taken into account—photoelectric effect, Compton scattering, and electron-positron pair generation. Simulation of electron trajectories was made according to the continuous slowing down approximation (CSDA) using Molière's theory of multiple scattering, which has been reported to provide satisfactory precision for spatial distribution of secondary electron absorbed energy in the absence of heavy-atom media (which is true for thermoluminiscent dosimeters). A positron slowed down below the termination threshold was considered as absorbed; at the site of the positron absorption, annihilation photons were considered to be released.

III.A. Monte Carlo Model for Photon Transport

Transport simulation algorithm for the chosen problem can be written in *C*- and *T*-kernels formalism. For primary particles (gamma rays), three interaction processes were taken into account—photoelectric effect, Compton scattering, and electron-positron pair generation:

$$C(E',\boldsymbol{\Omega}',\gamma\to,\boldsymbol{\Omega},\zeta|\boldsymbol{r}) = \frac{\Sigma_{ph}+\Sigma_{\mathrm{KN}}+\Sigma_{\kappa}}{\Sigma_t(\boldsymbol{r},E',\gamma)} \quad .$$

The photoelectric effect was treated as absorption of a photon with release of an electron with the same energy (generation of characteristic X-rays was neglected); the distribution of the deflection angle of the photoelectron $f_{ph}(\mu)$ was taken from the report by Hubbel and Veige.[9] We assumed the azimuthal angle of the photoelectron release uniform in $[0,2\pi)$:

$$\Sigma_{ph}(E',\boldsymbol{\Omega}',\gamma\to E,\boldsymbol{\Omega},\zeta|\boldsymbol{r}) = \Sigma_{ph}(\boldsymbol{r},E')\delta_{\zeta e}\delta(E-E')f_{ph}(\boldsymbol{\Omega}\boldsymbol{\Omega}') \quad ,$$

$$f_{ph}(\mu) \propto \frac{1-\mu^2}{(1-b\mu)^3}\times\left(\frac{1}{1-b\mu}+\frac{3-3\sqrt{1-b^2}-2b^2}{(1-b^2)^{3/2}}\right) \quad , \quad (10)$$

where $b=v/c$ is the relative velocity of an electron in speed of light units.

Compton scattering is treated as a process with two outgoing particles: scattered photon and electron. Applying Klein-Nishina's theory, one can get the generalized particle form of the Compton differential cross section:

$$\Sigma_{\mathrm{KN}}(E',\boldsymbol{\Omega}',\gamma\to E,\boldsymbol{\Omega},\zeta|\boldsymbol{r}) = \frac{r_0^2}{2}n_e(\boldsymbol{r})\left(f_{\mathrm{KN}}(E'\to E)\delta_{\zeta\gamma}\delta(\boldsymbol{\Omega}'\boldsymbol{\Omega}-\mu_\gamma) + f_{\mathrm{KN}}(E'\to E'-E)\delta_{\zeta e}\delta(\boldsymbol{\Omega}'\boldsymbol{\Omega}-\mu_e)\right) \quad ,$$

$$f_{\mathrm{KN}}(E'\to E) = \frac{\varepsilon}{E'^2}\left(\frac{E'}{E}+\frac{E}{E'}+\left(1-\frac{\varepsilon}{E}+\frac{\varepsilon}{E'}\right)^2-1\right) \quad ,$$

$$\mu_\gamma = \left(1 - \frac{\varepsilon}{E} + \frac{\varepsilon}{E'}\right),$$

$$\mu_e = \frac{1}{\sqrt{1 + (\varepsilon(2E'E - \varepsilon(E' - E)))/((E' - E)(E' + \varepsilon)^2)}} \quad , \tag{11}$$

where

ε = electron rest mass energy

r_0 = classical electron radius

n_e = electron density

θ_γ = deflection angle of scattered photon

θ_e = Compton electron

$\mu_\gamma = \cos\theta_\gamma$

$\mu_e = \cos\theta_e$.

Sampling Compton scattering according to the generalized particle concept multiplies the statistical weight of the particle by a factor of 2 because two particles actually appear in this process, and only one particle is simulated.

The pair production differential section was considered in the following:

$$\begin{aligned}\Sigma_\kappa(E', \mathbf{\Omega}', \gamma \to E, \mathbf{\Omega}, \zeta | \boldsymbol{r}) &= \Sigma_\kappa(\boldsymbol{r}, E')\Big((1 - P_\gamma(E', E_t^{e^+})) \\ &\times f_\kappa(E' \to E)\,\frac{1 - b^2}{4\pi(1 - b\mathbf{\Omega}\mathbf{\Omega}')^2}\,(\delta_{\zeta e} + \delta_{\zeta e^+}) \\ &+ 2P_\gamma(E', E_t^{e^+})\delta(E - \varepsilon)\,\frac{1}{4\pi}\,\delta_{\zeta\gamma}\Big)\ . \end{aligned} \tag{12}$$

Here, Σ_κ is the total pair production linear section, and $f_\kappa(E' \to E)$ is normalized pdf for electron or positron energy described by Hough.[10] The second element of the sum describes the annihilation of the positron in situ (if energy of this positron is lower than the termination threshold $E_t^{e^+}$), and

$$P_\gamma(E', E_t^{e^+}) = \int_0^{E_t^{e^+}} f_\kappa(E' \to E)\,\mathrm{d}E$$

is the probability of immediate (in situ) annihilation.

III.B. Monte Carlo Model for Electron and Positron Transport

Coulomb forces have the leading role in the interaction between charged particles and matter. The path lengths between interactions are small and the number of interactions is so great that analog sampling of an electron random walk, when a significant path is covered in condensed matter, seems to be impossible. That is the reason for the use of approximate models of electron transport when short path lengths are coupled into larger segments for computational time reduction. If the transition probability density for fixed path length is known, one can statistically choose phase coordinates at the end of a segment. These coordinates, in their own turn, could be used as the initial coordinates for the next procedure to be chosen. The consequence of coordinates, obtained in such manner, is called *enclosed trajectory*. The path length between two consequent collisions of enclosed trajectory is much longer than the physical distance between two real consequent interactions.

One of the approaches to the enclosed trajectory simulation is the use of the CSDA when the path length between two neighboring collisions on the enclosed trajectory and energy loss of charged particles is deterministic, and scattering angle is sampled according to the theory of multiple scattering. In some problems of secondary radiation field calculations, the simple and fast CSDA model with Molière's distribution for deflection angle proved, e.g., by Baranov,[11] to be sufficient. Mathematically, the CSDA model corresponds to energy and angular variable separation in a collision kernel with further consideration of the energy part as a truncated Taylor series. Relative energy loss η of electron on a segment of an enclosed trajectory may be taken fixed: $E_{n+1} = (1 - \eta)E_n$ (Ref. 11), and length of the segment is calculated using the step-difference model: $\ell_n = (1 - \eta)E_n/\beta(E_n)$, when $\beta(E) = \int_0^E \Sigma_s(E \to E')(E - E')\,\mathrm{d}E'$ is called stopping power. In *C*- and *T*-kernel formalism, it can be written as follows:

$$T(\boldsymbol{r}' \to \boldsymbol{r} | E, \mathbf{\Omega}, \zeta = e(e^+)) = \frac{\beta(\boldsymbol{r}, E, e(e^+))\delta\left(\eta E - \int_0^{|\boldsymbol{r} - \boldsymbol{r}'|} \beta(\boldsymbol{r}' + R\mathbf{\Omega} | E, e(e^+))\,\mathrm{d}R\right)\delta\left(\mathbf{\Omega} - \dfrac{\boldsymbol{r} - \boldsymbol{r}'}{|\boldsymbol{r} - \boldsymbol{r}'|}\right)}{|\boldsymbol{r} - \boldsymbol{r}'|^2} \tag{13}$$

and

$$C(E', \mathbf{\Omega}', \zeta = e(e^+) \to E, \mathbf{\Omega}, \zeta | \boldsymbol{r}) = \delta(E - E'(1 - \eta))f_{\mathrm{M}}(\mathbf{\Omega}\mathbf{\Omega}')\delta_{\zeta e(e^+)}\ . \tag{14}$$

Angular distribution is described by Molière's function, which is valid for multiple scattering on small angles (as far as reported by Bethe[12]):

$$f_M(\theta)\sin\theta\,d\theta = \left(2\exp(-\vartheta^2) + \frac{f_1(\vartheta)}{B} + \frac{f_2(\vartheta)}{B^2} + \ldots\right)\vartheta\,d\vartheta \ , \qquad (15)$$

where

θ = multiple scattering angle

$\vartheta = \theta/(\chi_C\sqrt{B})$

= effective scattering angle

$\chi_C = (22.9Z/pcb)\sqrt{\ell_m/A}$

= screening angle in degrees

Z = average atomic number of matter

A = average atomic mass

p = impulse of electron in rest mass energy units

b = relative velocity

ℓ_m = length of enclosed trajectory segment (g/cm^2).

Parameter B slightly changes with the average number of electron collisions (as mentioned by Baranov[11]), functions f_1 and f_2 are the first and second momenta of the distribution, respectively, defined and tabulated by Bethe.[12]

An electron slowed down under the termination threshold is considered to be absorbed, while a positron slowed down below the same threshold is considered to produce an annihilation photon pair. Thus, the collision kernel for positron annihilation can be written as follows:

$$C_{an}\left(\frac{E_t^{e^+}}{1-\eta} < E' \le E_t^{e^+}, \boldsymbol{\Omega}', e^+ \to E, \boldsymbol{\Omega}, \zeta\right) = \frac{2}{4\pi}\,\delta(E-\varepsilon)\delta_{\zeta\gamma} \ .$$

IV. ADJOINT COUPLED PHOTON-ELECTRON-POSITRON TRANSPORT SAMPLING IN CONTINUOUS SLOWING DOWN APPROXIMATION

IV.A. Detector Response Function, Total Cross Sections, and General Transition Probability Density Functions

Let us apply the Monte Carlo transport model described in Sec. III to adjoint simulation. When sampling adjoint transport, one must start the random walk in a detector rather than in a source. Detector function D is used for setting the initial point of an adjoint trajectory. This function depends upon the considered tally of the radiation field and can be represented as a weight factor that is integrated with forward flux through all phase space:

$$F = \langle \varphi(\boldsymbol{r}, E, \boldsymbol{\Omega}, \zeta), D(\boldsymbol{r}, E, \boldsymbol{\Omega}, \zeta)\rangle \ .$$

So, for calculations of flux, the detector function has the simplest form: It is constant, and the initial adjoint particle energy is distributed uniformly.

Now one can define the detector function for energy absorption. The absorbed energy is connected with generation of a particle with energy lower than the termination threshold E_t^{ζ}. When a particle of type zeta reaches this threshold, it is considered to be absorbed, and the Monte Carlo story terminates. For photons, energy absorption takes place through the photoelectric effect, Compton scattering, and pair production while the expected contribution from one collision is:

$$\tilde{D}(\boldsymbol{r}, E, \boldsymbol{\Omega}, \gamma) = \sum_{\zeta'=\gamma,e,e^+}\int_0^E E' H(E_t^{\zeta'} - E')\,C(E, \boldsymbol{\Omega}, \zeta \to E', \boldsymbol{\Omega}', \zeta' \,|\, \boldsymbol{r})\,dE'\,d\boldsymbol{\Omega}'$$

$$= \frac{1}{\Sigma_t(\boldsymbol{r}, E)}\left(2\pi\,\frac{r_0^2}{2}\,n_e(\boldsymbol{r})\int_0^E (E' H(E_t^{\gamma} - E') + (E - E')H(E_t^{e} - E + E'))f_{KN}(E \to E')\,dE'\right.$$

$$\left. + \Sigma_{ph}(\boldsymbol{r}, E)EH(E_t^e - E) + 2\Sigma_{\kappa}(\boldsymbol{r}, E)\int_0^{E_t^e} E' f_{\kappa}(E \to E')\,dE'\right) \ , \qquad (16)$$

where $H(\ldots)$ is the Heaviside function. Taking into account the relationship (see Ref. 3) $\tilde{D} = D/\Sigma_t$, one can define scoring from unit path length D, which is used as an adjoint source function:

$$D(\boldsymbol{r}, E, \boldsymbol{\Omega}, \gamma) = \tilde{D}(\boldsymbol{r}, E, \boldsymbol{\Omega}, \gamma)\Sigma_t(\boldsymbol{r}, E, \gamma) \ . \qquad (17)$$

As to electrons and positrons, Halbleib and Morel[1] mentioned that the stopping power $\beta(\boldsymbol{r}, E)$ has the meaning of direct contribution to energy absorption from unit path length $D(\boldsymbol{r}, E, \boldsymbol{\Omega}, e(e^+)) = \beta(\boldsymbol{r}, E, e(e^+))$. From the other side, the direct contribution from one collision of electron or positron on an enclosed trajectory is $\tilde{D}(\boldsymbol{r}, E, e(e^+)) = \eta E$. Then it is possible to define the effective total cross section for electrons and positrons according to the enclosed trajectory concept:

$$\Sigma_t(\boldsymbol{r}, E, e(e^+)) = \frac{\beta(\boldsymbol{r}, E, e(e^+))}{\eta E} \quad ; \tag{18}$$

the effective Molière's differential cross section:

$$\Sigma(E', \boldsymbol{\Omega}', e(e^+) \to E, \boldsymbol{\Omega}, \zeta | \boldsymbol{r}) = \frac{\beta(\boldsymbol{r}, E', e(e^+))}{\eta E'} \delta(E - E'(1-\eta)) \times f_{\mathrm{M}}(\boldsymbol{\Omega}\boldsymbol{\Omega}') \delta_{\zeta e(e^+)} \quad ; \tag{19}$$

as well as the effective positron annihilation cross section:

$$\Sigma_{an}(E, \zeta = e^+ \to \varepsilon, \zeta = \gamma | \boldsymbol{r}) = C_{an}(E, e^+ \to \varepsilon, \gamma | \boldsymbol{r}) \frac{\beta(\boldsymbol{r}, E, e^+)}{\eta E} \quad . \tag{20}$$

Different tallies need different detector functions to be used. For example, the detector function for current through the certain surface is

$$D(\boldsymbol{r}, E, \boldsymbol{\Omega}, e(e^+)) = \delta_s(\boldsymbol{r}) |\boldsymbol{n}(\boldsymbol{r}), \boldsymbol{\Omega}| \quad , \tag{21}$$

where the surface indicator function δ_s is zero everywhere except at the surface while the integral from this function through all the transport volume is equal to the surface area, and $\boldsymbol{n}$ is the normal vector to the surface.

According to the generalized particle formalism and the cross sections defined in Sec. III, the following interaction channels for an adjoint particle entering a collision in phase point $\boldsymbol{r}, E, \boldsymbol{\Omega}, \zeta$, can be described.

IV.B. Collision Kernel Sampling for Adjoint Photons

For adjoint annihilation radiation (which has emerged either from regular-singular transition or directly in the adjoint source when a history starts from the singular state and, therefore, has $\zeta' = \gamma$, $E' = \varepsilon$), two scattering channels exist:

1. conversion to an adjoint positron with energy between termination threshold $E_t^{e^+}$ and $E_t^{e^+}/(1-\eta)$:

$$C^+_{an\,e^+}(\varepsilon, \boldsymbol{\Omega}', \gamma \to E, \boldsymbol{\Omega}, \zeta | \boldsymbol{r}) = \frac{\beta(\boldsymbol{r}, E, e^+)}{\eta E \Sigma_t(\boldsymbol{r}, \varepsilon)} 2H(E - E_t^{e^+}) \times H\left(\frac{E_t^{e^+}}{1-\eta} - E\right) \frac{1}{4\pi} \delta_{\zeta e^+} \quad , \tag{22}$$

2. conversion to an adjoint photon (positron annihilation in situ):

$$C^+_{an\,\gamma}(\varepsilon, \boldsymbol{\Omega}', \gamma \to E, \boldsymbol{\Omega}, \zeta | \boldsymbol{r}) = 2P_\gamma(E, E_t^{e^+}) \frac{\Sigma_\kappa(\boldsymbol{r}, E)}{\Sigma_t(\boldsymbol{r}, \varepsilon)} \frac{1}{4\pi} \delta_{\zeta\gamma} \quad . \tag{23}$$

Probabilities of realization for these channels during Monte Carlo sampling are proportional to $P_{an\,e^+}$ and $P_{an\,\gamma}$, i.e., the integrals from these kernels along the outgoing arguments. The direction of outgoing adjoint positron (or photon) is isotropic.

For regular adjoint photons with energies $E' \neq \varepsilon$, the possible interaction channels are as follows:

1. regular adjoint Compton effect:

$$C^+_{\mathrm{KN}\,reg}(E', \boldsymbol{\Omega}', \gamma \to E, \boldsymbol{\Omega}, \zeta | \boldsymbol{r}) = \frac{r_0^2 n_e(\boldsymbol{r})}{2\Sigma_t(\boldsymbol{r}, E')} \frac{\varepsilon}{E^2} \times \left(\frac{E}{E'} + \frac{E'}{E} + \left(1 - \frac{\varepsilon}{E'} + \frac{\varepsilon}{E}\right)^2 - 1\right) \times \delta\left(\boldsymbol{\Omega}\boldsymbol{\Omega}' - \left(1 - \frac{\varepsilon}{E'} + \frac{\varepsilon}{E}\right)\right) \delta_{\zeta\gamma} \quad , \tag{24}$$

2. singular adjoint Compton effect, possible when $\varepsilon/3 < E' < \varepsilon$:

$$C^+_{\mathrm{KN}\,sing}(E', \boldsymbol{\Omega}', \gamma \to E, \boldsymbol{\Omega}, \zeta | \boldsymbol{r}) = C^+_{\mathrm{KN}\,reg}(E', \boldsymbol{\Omega}', \gamma \to E, \boldsymbol{\Omega}, \zeta | \boldsymbol{r}) \delta(E - \varepsilon) \quad . \tag{25}$$

For the regular adjoint Compton effect, if $E' \geq \varepsilon/2$, the upper limit of E does not exist and the total integral through all the outgoing energies logarithmically diverges. However, when the source has a finite spectrum, the upper energy limit is also finite; that is sufficient for proper normalization (adjoint photons with energies higher than the maximal source energy have no importance and need not be simulated).

To simulate the transposed Klein-Nishina function, the technique suggested by Koblinger[13] was used. This technique assumes biasing C^+-kernel by multiplying the factor E'/E. The integral from E' up to infinity of the biased kernel becomes limited. After the integral becomes limited, the adjoint outgoing energy E can be sampled from the pdf for the undimensioned variable $y = E'/E$, which designates the ratio of scattered and unscattered photon energies and is proportional to

$$f^+_{\mathrm{KN}\gamma}(y) = (\phi_1(y) + \phi_2(y) + \phi_3(y)) \quad ,$$

$$y_{min} \leq y \leq 1 \quad , \quad y_{min} = \begin{cases} 1 - 2\alpha' & \alpha' < \frac{1}{2} \\ 0 & \alpha' \geq \frac{1}{2} \end{cases} \quad ,$$

$$\phi_1(y) = 1 - y \quad , \quad \phi_2(y) = y^2 \quad ,$$

$$\phi_3(y) = \frac{\alpha' + y - 1}{\alpha'^2} \quad , \quad \alpha' = E'/\varepsilon \quad . \tag{26}$$

After obtaining outgoing energy E, the statistical weight of the adjoint particle must be multiplied by the correction factor:

$$W_{C^+} = \frac{\pi r_0^2 n_e(\boldsymbol{r}) \varepsilon I^+_{\mathrm{KN}\gamma}}{E' \Sigma_t(\boldsymbol{r}, E')} \frac{E}{E'} \ , \tag{27}$$

where $I^+_{\mathrm{KN}\gamma}$ is the integral from $f^+_{\mathrm{KN}\gamma}$ through all possible y.

The scattering angle μ_γ for the adjoint Compton effect is $\mu_\gamma = \boldsymbol{\Omega}\boldsymbol{\Omega}' - (1 - \varepsilon/E' + \varepsilon/E)$. The azimuthal scattering angle is taken uniform in $[0, 2\pi)$ for all types of scattering in our work.

The probabilities for realization of regular and singular channels are proportional to

$$P_{reg} = \pi r_0^2 n_e(\boldsymbol{r}) \varepsilon I^+_{\mathrm{KN}\gamma}(E')/(E' \Sigma_t(\boldsymbol{r}, E'))$$

and

$$P_{sing} = \pi r_0^2 n_e(\boldsymbol{r}) \varepsilon f_{\mathrm{KN}}(\varepsilon \to E') \times (P_{an\, e^+} + P_{an\, \gamma})/\Sigma_t(\boldsymbol{r}, E') \ ,$$

respectively. In the singular case, the outgoing adjoint photon energy is set to ε, and the scattering angle cosine is set to $2 - \varepsilon/E'$.

IV.C. Collision Kernel Sampling for Adjoint Charged Particles

In forward simulation, an electron can emerge from the following types of interaction: Compton effect, photoelectric absorption, pair production, and electron multiple scattering according to the CSDA model. Thus, for adjoint electrons entering a collision, the following interaction channels are possible:

1. regular adjoint Compton effect:

$$C^+_{\mathrm{KN}\ reg}(E', \boldsymbol{\Omega}', e \to E, \boldsymbol{\Omega}, \zeta | \boldsymbol{r}) = \frac{r_0^2 n_e(\boldsymbol{r}) \eta E'}{2\beta(\boldsymbol{r}, E', e)} \frac{\varepsilon}{E^2} \left(\frac{E}{E - E'} + \frac{E - E'}{E} + \left(1 - \frac{\varepsilon}{E - E'} + \frac{\varepsilon}{E} \right)^2 - 1 \right) \times \delta \left(\boldsymbol{\Omega}\boldsymbol{\Omega}' - \frac{1}{\sqrt{1 + (\varepsilon(2E^2 - E'(2E + \varepsilon)))/(E'(E + \varepsilon)^2)}} \right) \delta_{\zeta\gamma} \ , \tag{28}$$

2. singular adjoint Compton effect, possible when $E' < \frac{2}{3}\varepsilon$:

$$C^+_{\mathrm{KN}\ sing}(E', \boldsymbol{\Omega}', e \to E, \boldsymbol{\Omega}, \zeta | \boldsymbol{r}) = C^+_{\mathrm{KN}\ reg}(E', \boldsymbol{\Omega}', e \to E, \boldsymbol{\Omega}, \zeta | \boldsymbol{r}) \delta(E - \varepsilon) \ , \tag{29}$$

3. regular adjoint photoelectric effect:

$$C^+_{ph\ reg}(E', \boldsymbol{\Omega}', e \to E, \boldsymbol{\Omega}, \zeta | \boldsymbol{r}) = \frac{\Sigma_{ph}(\boldsymbol{r}, E') \eta E'}{\beta(\boldsymbol{r}, E')} \delta_{\zeta\gamma} \delta(E - E') f_{ph}(\boldsymbol{\Omega}\boldsymbol{\Omega}') \ , \tag{30}$$

where $f_{ph}(\ldots)$ is the self-adjoint photoelectric angular pdf,

4. singular adjoint photoelectric effect, possible when $(1 - \eta)\varepsilon < E' \le \varepsilon$:

$$C^+_{ph\ sing}(\varepsilon(1 - \eta) < E' \le \varepsilon, \boldsymbol{\Omega}', e \to E, \boldsymbol{\Omega}, \zeta | \boldsymbol{r}) = \frac{\Sigma_{ph}(\boldsymbol{r}, \varepsilon)}{\beta(\boldsymbol{r}, E')} \delta_{\zeta\gamma} \delta(E - \varepsilon) f_{ph}(\boldsymbol{\Omega}\boldsymbol{\Omega}') \ , \tag{31}$$

5. adjoint pair production:

$$C^+_{\kappa}(E', \boldsymbol{\Omega}', e \to E, \boldsymbol{\Omega}, \zeta | \boldsymbol{r}) = \frac{\Sigma_{\kappa}(E, \boldsymbol{\Omega}, \gamma \to E', \boldsymbol{\Omega}', e | \boldsymbol{r}) \delta_{\zeta\gamma} \eta E'}{\beta(\boldsymbol{r}, E', e)} \ , \tag{32}$$

6. gaining energy in model adjoint to CSDA:

$$C^+_{\mathrm{CSDA}}(E', \boldsymbol{\Omega}', e \to E, \boldsymbol{\Omega}, \zeta | \boldsymbol{r}) = \frac{\eta E'}{\eta E} \frac{\beta(\boldsymbol{r}, E, e)}{\beta(\boldsymbol{r}, E', e)} \delta(E' - E(1 - \eta)) f_{\mathrm{M}}(\boldsymbol{\Omega}\boldsymbol{\Omega}') \delta_{\zeta e} = \frac{\beta(\boldsymbol{r}, E, e)}{\beta(\boldsymbol{r}, E', e)} \delta \left(E - \frac{E'}{1 - \eta} \right) f_{\mathrm{M}}(\boldsymbol{\Omega}\boldsymbol{\Omega}') \delta_{\zeta e} \ , \tag{33}$$

where $f_{\mathrm{M}}(\ldots)$ is the self-adjoint Molière's angular pdf.

The last two channels are regular and are possible not only for adjoint electrons but also for adjoint positrons.

For sampling the regular adjoint Compton effect for incoming adjoint electrons, the outgoing energy is equal to

$$E_{min} \le E < \infty \ , \quad E_{min} = (E' + \sqrt{E'^2 + 2\varepsilon E'})/2 \ ,$$

where the lower limit E_{min} corresponds to the zero electron deflection angle ($\mu_e = 1$) and strict backscattering for the photon ($\mu_\gamma = -1$).

Fortunately, the transposed Klein-Nishina cross section for adjoint electrons can be normalized (the integral from this section through all the possible energies up to infinity does not diverge). We developed a special simulation algorithm for the Compton effect and entering adjoint electron. Denoting (as in Sec. IV.B) by $y = (E - E')/E$ the ratio between photon energies before and after scattering, one will have the following distribution for y:

$$C^+_{\mathrm{KN}e}(y|\boldsymbol{r}, E', e) = \frac{\pi r_0^2 n_e(\boldsymbol{r})\eta E'}{\beta(\boldsymbol{r}, E', e)} \frac{\varepsilon}{E'} \times \left(y + \frac{1}{y} + \left(1 - \frac{(1-y)^2 \varepsilon}{yE'} \right)^2 - 1 \right) . \quad (34)$$

The pdf for y can be expressed as a sum of the truncated Laurent series and is proportional to

$$f^+_{\mathrm{KN}e}(y) = \sum_{i=-2}^{2} C_i y^i \ , \quad C_{-2} = C_2 = t^2 \ ,$$
$$C_{-1} = C_1 = 1 - 2t - 4t^2 \ , \quad C_0 = 4t + 6t^2 \ ,$$
$$t = \frac{\varepsilon}{E'} \ . \quad (35)$$

The value y was sampled by the superposition method in the segment $[y_{min}, y_{max}]$, where $y_{min} = 1/(1 + (E' + \sqrt{E'^2 + 2\varepsilon E'})/\varepsilon)$, $y_{max} = 1 - E'/E_{max}$, and E_{max} is the maximal source energy. The probability of realization for this interaction channel is proportional to the total integral from the adjoint electron Compton scattering and is equal to

$$P^+_{\mathrm{KN}e\ reg}(\boldsymbol{r}, E', e) = \frac{\pi r_0^2 n_e(\boldsymbol{r})\eta E'}{\beta(\boldsymbol{r}, E', e)} \frac{\varepsilon}{E'} I^+_{\mathrm{KN}e} \ , \quad (36)$$

where $I^+_{\mathrm{KN}e}$ is the integral from $f^+_{\mathrm{KN}e}$ through all possible y.

When sampling the singular transposed Compton effect for adjoint electrons, one must set the outgoing energy E to ε, and the scattering angle cosine is set to

$$\boldsymbol{\Omega}\boldsymbol{\Omega}' = \frac{1}{\sqrt{1 + \dfrac{2\varepsilon - 3E'}{4E'}}} \ .$$

The probability of realization for the singular Compton effect is proportional to

$$P^+_{\mathrm{KN}e\ sing} = \pi r_0^2 n_e(\boldsymbol{r}) \varepsilon f_{\mathrm{KN}}(\varepsilon \to \varepsilon - E') \times \eta E' (P_{an\ e^+} + P_{an\ \gamma})/\beta(\boldsymbol{r}, E', e) \ .$$

Since the photoelectric effect model generates only one particle, a photoelectron with energy of an absorbed photon, the photoelectric cross section is almost self-adjoint:

$$C^+_{ph}(E', \boldsymbol{\Omega}', e \to E, \boldsymbol{\Omega}, \zeta|\boldsymbol{r}) = \frac{\Sigma_{ph}(\boldsymbol{r}, E')\eta E'}{\beta(\boldsymbol{r}, E')} \delta_{\zeta\gamma} \delta(E - E') f_{ph}(\boldsymbol{\Omega}\boldsymbol{\Omega}') \ . \quad (37)$$

The difference between the forward and the adjoint photoelectric sections consists of incoming and outgoing particle-type transposition only. The angular transition pdf is self-adjoint and was given in Eq. (10). This distribution function can be sampled, e.g., from tables calculated before Monte Carlo histories simulation. The total integral from the adjoint photoelectric effect is

$$P^+_{ph}(\boldsymbol{r}, E') = (\Sigma_{ph}(\boldsymbol{r}, E')\eta E')/\beta(\boldsymbol{r}, E', e) \ . \quad (38)$$

During the singular adjoint photoelectric effect, which probability is proportional to $P^+_{ph\ sing}(\boldsymbol{r}, E') = \Sigma_{ph}(\boldsymbol{r}, \varepsilon)(P_{an\ e^+} + P_{an\ \gamma})/\beta(\boldsymbol{r}, E', e)$, the outgoing photon energy is set to ε, and the scattering angle is simulated as in the regular photoelectric effect.

The transposed pair generation process for incoming adjoint electrons and positrons was described by Bethe-Geitler's theory using the following equation:

$$C^+_{\kappa}(E', \boldsymbol{\Omega}', \zeta = e(e^+) \to E, \boldsymbol{\Omega}, \zeta|\boldsymbol{r}) = \frac{\Sigma_{\kappa}(\boldsymbol{r}, E)\eta E'}{\beta(\boldsymbol{r}, E')} (1 - P_{\gamma}(E, E_t^+)) \times f_{\kappa}(E \to E') \frac{1 - b'^2}{4\pi(1 - b'\boldsymbol{\Omega}\boldsymbol{\Omega}')^2} \delta_{\zeta\gamma} \ . \quad (39)$$

The probability of this process is proportional to the integral from Eq. (39) along the outgoing arguments. The polar deflection angle cosine was sampled according to Eq. (39) as

$$\mu = \frac{1 - 2\xi + b}{1 + b - 2b\xi} \ ,$$

where ξ is uniformly distributed on $[0,1)$ random number.

The following function describes multiple scattering and energy gain in adjoint CSDA models for electrons and positrons:

$$C^+_{\mathrm{CSDA}}(E', \boldsymbol{\Omega}', e(e^+) \to E, \boldsymbol{\Omega}, \zeta|\boldsymbol{r}) = \frac{\eta E'}{\eta E} \frac{\beta(\boldsymbol{r}, E, e(e^+))}{\beta(\mathbf{r}, E', e(e^+))} \times \delta(E' - E(1 - \eta)) f_{\mathrm{M}}(\boldsymbol{\Omega}\boldsymbol{\Omega}') \delta_{\zeta e(e^+)} = \frac{\beta(\boldsymbol{r}, E, e(e^+))}{\beta(\boldsymbol{r}, E', e(e^+))} \delta\left(E - \frac{E'}{1 - \eta} \right) f_{\mathrm{M}}(\boldsymbol{\Omega}\boldsymbol{\Omega}') \delta_{\zeta e(e^+)} \ . \quad (40)$$

Molière's angular distribution is self-adjoint. The total integral from adjoint electron CSDA scattering is equal to

$$P^{+}_{\mathrm{CSDA}}(\boldsymbol{r}, E', \zeta = e(e^{+})) = \beta(\boldsymbol{r}, E, \zeta = e(e^{+}))/\beta(\boldsymbol{r}, E', \zeta = e(e^{+})) \ , \quad (41)$$

because the total CSDA operator is not self-adjoint. (This result has been obtained in another manner by Halbleib and Morel[1]).

Forward photon, electron, and positron interaction channels for this model are shown in Fig. 2a, and adjoint interaction channels are shown in Fig. 2b. Different channels correspond to different pdfs rather than physical events.

V. CALCULATION RESULTS AND DISCUSSION

To verify the validity and efficiency of the adjoint simulation algorithm described in this paper, calculations in parallel barrier geometry have been done. The source of primary gamma rays was located in one of the barrier boundaries. Major attention was paid to transport in thin slabs, where taking into account electron and positron transport is essential for calculation of absorbed energy spatial distribution. To increase the efficiency of photon transport simulation, photon transport was considered only within the slab (the escape was forbidden), which was realized with transport kernel biasing and statistical weight correction.

V.A. Validation of Transport Model

The validity of the transport model was checked by comparison between experiments measured by Wall and Burke[14] and calculated with forward Monte Carlo method dependence on energy absorption intensity upon the penetration depth in aluminum near the aluminum-gold interface (see Fig. 3). The monodirected flux of ^{60}Co gamma rays, incident to the right side of Fig. 3, was used as the

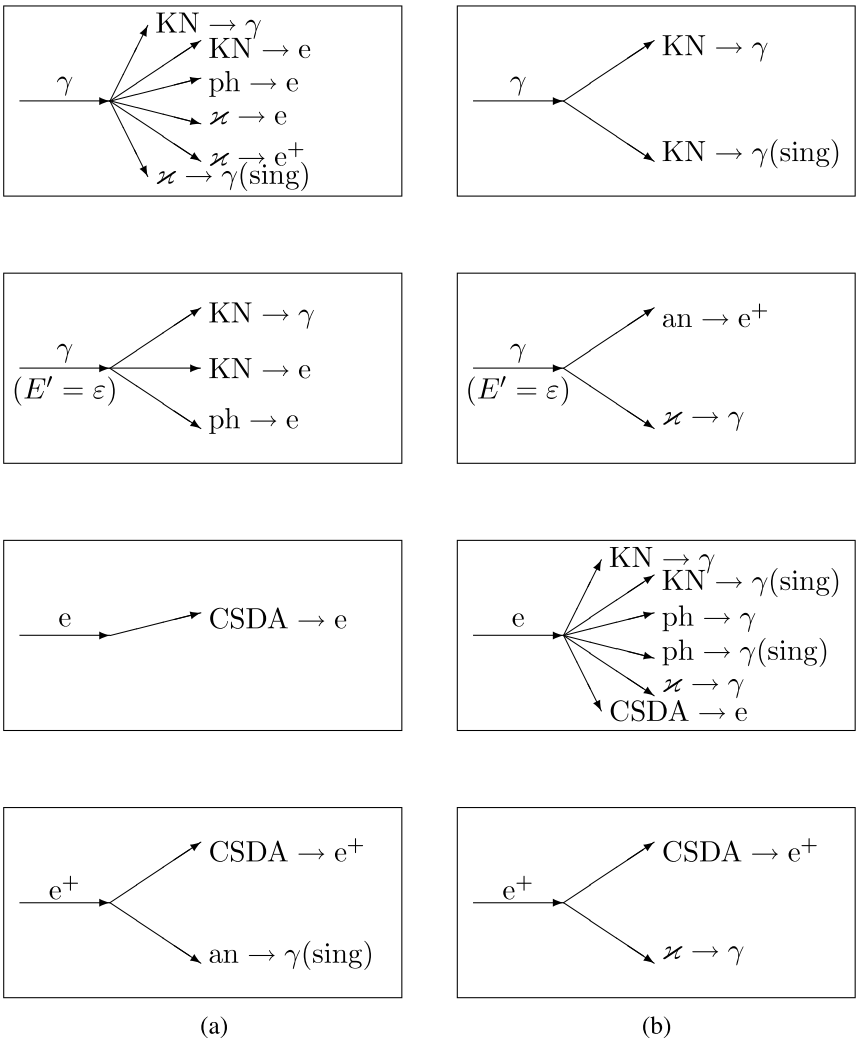

Fig. 2. Possible scattering channels for (a) forward and (b) adjoint particles.

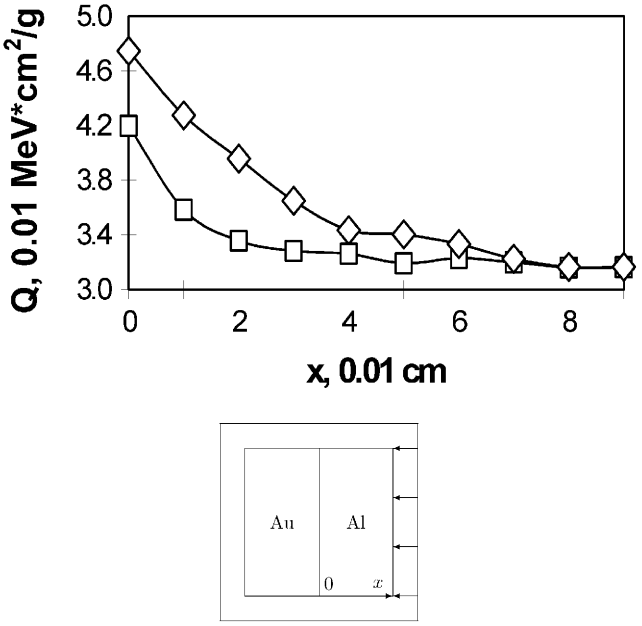

Fig. 3. Calculation (□) and experimental (◇) absorbed energy in aluminum near aluminum-gold interface from exposition of ^{60}Co gamma rays, incident from the right side of aluminum slab (as shown on small scheme below).

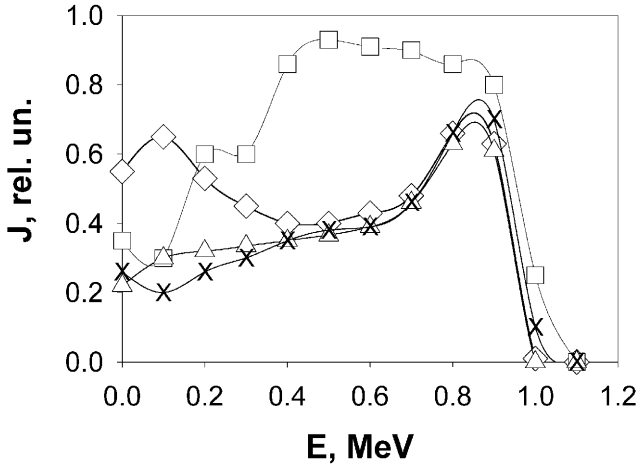

Fig. 4. Secondary electron current spectra from ^{60}Co gamma ray source in thin light-matter slab [◇ = water slab, CSDA model, presence of lead slab behind; □ = X-ray film, simulation of delta electrons, presence of lead slab behind (taken from Ref. 15); △ = water slab, CSDA model, absence of lead slab behind; × = X-ray film, simulation of delta electrons, absence of lead slab behind (taken from Ref. 15)].

source. The coordinate $x = 0$ corresponds to the exact position of the aluminum-gold interface. The difference in the rate of electron equilibrium formation between calculation and experiment is likely to be caused by the absence of delta-electron simulation in CSDA. However, in heavy materials such as gold, the generation of delta electrons, which eventually appear in aluminum, is essential.

The adequacy of the CSDA model for light media and inadequacy for heavy media are clearly shown in the spectral analysis of secondary electrons for the following problem. The monodirected flux of ^{60}Co gamma rays was incident to the thin (4-mm) light-matter slab. Behind the light-matter slab, there could be a heavy-matter (lead) slab of 2 mm thickness. The secondary electron current spectrum at the surface located at 3 mm from the source for the CSDA model and water slab, as well as for the Monte Carlo model with delta-electron track simulation,[15] is shown in Fig. 4. The spectra calculated according to CSDA and simulation of delta electrons are almost identical in the absence of lead, while the spectra in the presence of lead are considerably different.

V.B. Validation of Adjoint Simulation According to Generalized Particle Concept

For adjoint calculations with a monoenergetic ($E = E_0$) source, the special adjoint estimator, local in the energy-phase coordinate, was developed. The estimator used convolution with function proportional to the first outgoing collision density. For the planar source with arbitrary polar angle distribution $S(\mathbf{\Omega}) = S(\Omega_x)/2\pi$, where x is the axis normal to the source plane, the first incoming collision density is

$$\psi_1(\boldsymbol{r}, E, \mathbf{\Omega}, \zeta) = \frac{S(\Omega_x)\Sigma_t(E_0)}{2\pi\Omega_x} \times \exp\left(-\frac{\Sigma_t(E_0)x}{\Omega_x}\right)\delta(E - E_0)\delta_{\zeta\gamma} \ ,$$

and the first outgoing collision density is

$$\chi_1(\boldsymbol{r}, E, \mathbf{\Omega}, \zeta) = \frac{1}{2\pi}\int \Sigma(E_0, \mathbf{\Omega}', \gamma \to E, \mathbf{\Omega}, \zeta|\boldsymbol{r})\,\frac{S(\Omega'_x)}{\Omega'_x} \times \exp\left(-\frac{\Sigma_t(E_0)x}{\Omega'_x}\right)\mathrm{d}\mathbf{\Omega}' \ .$$

This integral was calculated with Monte Carlo methods, taking into account the dependence on the forward collision kernel (see Sec. III.A).

Because of modeling adjoint collision-density–like functions χ^+ and ψ^+ rather than fluxlike functions χ^* and ψ^*, one should use as an estimator the forward fluxlike value equal to χ_1/Σ_t.

For photoelectric absorption, the first outgoing collision density also has a delta-function factor in the energy part ($E = E_0$). However, it can be estimated with the score, equal to

TABLE I

Absorbed Energy Dependence upon Penetration Depth for Monoenergetic (1 MeV) Isotropic Source Located in Slab Boundary for Different Modifications of Monte Carlo Method

Depth (10^{-2} mfp)	Forward Analog	Forward Generalized	Adjoint	FOM
Scattered photons, 10^{-5} MeV per source photon per subslab				
0.05	1.28 ± 2%	1.25 ± 3%	1.5 ± 13%	1.5
0.15	1.27 ± 2%	1.27 ± 3%	1.30 ± 5%	9.1
0.25	1.37 ± 2%	1.30 ± 3%	1.27 ± 5%	11
0.35	1.37 ± 2%	1.36 ± 3%	1.29 ± 4%	14
0.45	1.38 ± 2%	1.39 ± 4%	1.22 ± 4%	14
0.55	1.33 ± 2%	1.40 ± 3%	1.23 ± 4%	13
0.65	1.37 ± 2%	1.34 ± 3%	1.33 ± 4%	15
0.75	1.30 ± 2%	1.29 ± 3%	1.24 ± 5%	7.0
0.85	1.28 ± 2%	1.30 ± 2%	1.27 ± 6%	5.6
0.95	1.23 ± 2%	1.20 ± 2%	1.17 ± 5%	8.8
Whole slab	13.2 ± 0.7%	13.1 ± 1.0%	12.8 ± 2%	0.57
Electrons, 10^{-3} MeV per source photon per subslab				
0.05	1.11 ± 1.1%	1.10 ± 1.5%	1.03 ± 3%	7.7
0.15	1.45 ± 0.9%	1.40 ± 1.3%	1.36 ± 2%	15
0.25	1.59 ± 0.8%	1.57 ± 1.2%	1.53 ± 2%	14
0.35	1.66 ± 0.7%	1.64 ± 1.1%	1.61 ± 2%	13
0.45	1.70 ± 0.6%	1.70 ± 1.0%	1.70 ± 2%	7.0
0.55	1.70 ± 0.7%	1.68 ± 1.0%	1.67 ± 1.3%	14
0.65	1.66 ± 0.6%	1.66 ± 1.0%	1.58 ± 1.1%	18
0.75	1.59 ± 0.6%	1.59 ± 1.0%	1.52 ± 1.5%	9.1
0.85	1.47 ± 0.6%	1.49 ± 0.9%	1.45 ± 1.1%	17
0.95	1.26 ± 0.6%	1.28 ± 0.9%	1.24 ± 1.4%	10
Whole slab	15.2 ± 0.3%	15.1 ± 0.5%	14.7 ± 0.5%	2.3

$$\frac{\Sigma_{ph}(E_0)}{2\pi\beta(E,e)} \int f_{ph}(\mathbf{\Omega}\mathbf{\Omega}') \frac{S(\Omega'_x)}{\Omega'_x} \times \exp\left(-\frac{\Sigma_t(E_0)x}{\Omega'_x}\right) d\mathbf{\Omega}' \ ,$$

calculated when $\zeta = e$, $E_0/(1-\eta) < E \le E_0$.

Algorithms for simulation of adjoint regular collision kernels were tested for the following problem: monoenergetic (1 MeV) and isotropic source, water slab with width of 0.01 mean free path (mfp), termination threshold for photons 25 keV, for electrons 250 keV (for lower termination thresholds Molière's theory does not work properly), and relative energy loss η on enclosed trajectory segment 6%. The photon was considered to produce a contribution when it could produce an underthreshold particle; the electron was considered to produce a contribution when it loses energy in the CSDA model. Fractions of absorbed energy from unscattered photons, scattered photons, and electrons were calculated separately.

Calculation results for three modifications of the Monte Carlo method were compared:

1. analog forward calculations where particles generated in the transport process were followed up to every termination

2. forward generalized particle method described in Sec. III

3. adjoint generalized particle method described in Sec. IV.

The results are shown in Table I. The relative error shown is 1σ. The efficiencies [figure of merit (FOM)] of forward analog and forward generalized particle methods are approximately equal to each other. Run-time ratio designates the relative adjoint FOM (forward FOM is taken to be 1). For thin subslab zones, the adjoint method efficiency is an order greater than for the forward one. Total tallies that represent energy absorption in the whole slab (10 times thicker) are not as convenient for the adjoint method.

The dependence of energy absorption upon penetration depth (expressed in mega-electron-volt per source photon per subslab) is shown in Fig. 5. In the left side of the diagram, one can clearly observe the gradual forming of electron equilibrium; in the right side, one can observe the attenuation of radiation with large incident angles.

To verify the adjoint simulation algorithm for fixed-energy states, we made a comparison of the results for

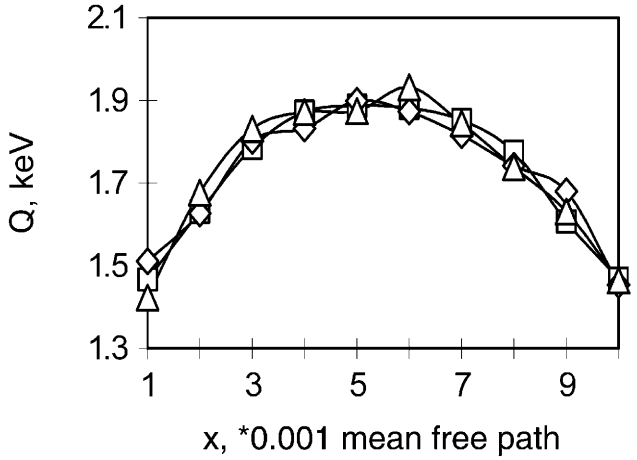

Fig. 5. Spatial distribution of total energy absorption upon penetration depth (expressed in keV per subslab per source photon) in thin water slab for monoenergetic (1 MeV) isotropic source located in slab boundary for different modifications of Monte Carlo method (□ = forward analog method; ◇ = forward generalized particle method; △ = adjoint generalized particle method).

TABLE II

Absorbed Energy in Slab, MeV per Source Photon for 9-MeV Gamma Ray Isotropic Source, Located at the Boundary of 0.01 mfp Water Slab

Particle and Energy	Forward Method	Adjoint Method	Relative FOM
γ, $E = 0.511$ MeV	$4.26 \times 10^{-5} \pm 1.0\%$	$4.28 \times 10^{-5} \pm 2\%$	0.6
γ, $E < 0.511$ MeV	$4.72 \times 10^{-6} \pm 3\%$	$4.74 \times 10^{-6} \pm 3\%$	1.0
e, $E < 0.511$ MeV	$5.21 \times 10^{-5} \pm 3\%$	$4.94 \times 10^{-5} \pm 2\%$	2.8

forward and adjoint Monte Carlo calculations of absorbed energy in a thin (0.01 mfp) water slab. A photon 9-MeV planar isotropic source was located at the boundary of the slab. Absorbed energy from annihilation radiation and particles generated by it are shown in Table II. The relative error indicates 1σ, so forward and adjoint results are statistically similar. The relative FOM indicates the ratio of adjoint FOM to forward FOM. In thin subslabs (ten times thinner than a whole slab), the relative efficiency of the adjoint method is higher because of detector localization.

Spectral currents of secondary electrons and positrons for the surface, located at 0.0075 mfp's from the frontal surface, are shown in Fig. 6. The calculations were done by Monte Carlo according to previously defined forward and adjoint transport modes. The discrepancy between forward and adjoint results in each spectral channel lies within the statistical error bar (which corresponds to 2σ) for each channel.

Thus, one can conclude that the spatial distribution of absorbed energy and the energy spectra of secondary particles prove the adequacy of the introduced coupled gamma-ray–electron–positron transport model for light media.

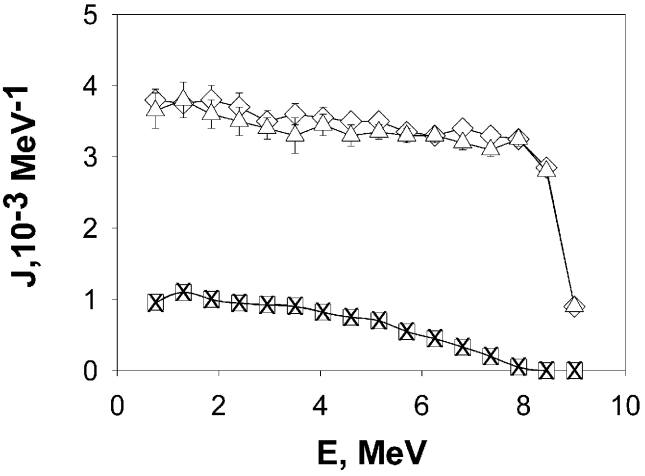

Fig. 6. Secondary electron and positron current spectra (expressed in MeV^{-1} per source photon) from 9-MeV gamma-ray source in thin (0.01 mfp's) water slab near at 0.0075 mfp's from the front ($\diamond$ = forward method for electrons; $\square$ = forward method for positrons; $\triangle$ = adjoint method for electrons; $\times$ = adjoint method for positrons).

VI. CONCLUSION

The generalized particle concept, based on phase-space extension with an additional discrete coordinate, the particle type, was developed and mathematically grounded. With the use of developed concept, a new approach to the adjoint transport equation simulation for coupled transport of particles with different type was proposed. The generalized particle Monte Carlo approach assumes simulation of only one particle outgoing from the collision even for processes with multiple particles outgoing from this collision, which does not require splitting in forward simulation algorithm and also allows adjoint Monte Carlo simulation. Moreover, the generalized particle concept allows implementation of fixed-energy secondary radiation (as singular state) into adjoint transport calculations. The applicability of the generalized particle concept to the adjoint Monte Carlo method was demonstrated on the example of the coupled gamma-ray–electron–positron transport problem with CSDA for charged particles, which is adequate for the absence of heavy media. In thin slabs due to small detector extension, adjoint methods are more effective then forward methods.

REFERENCES

1. J. A. HALBLEIB and J. E. MOREL, "Adjoint Monte Carlo Electron Transport in the Continuous-Slowing-Down Approximation," *J. Comput. Phys.*, **43**, 211 (1980).

2. J. A. HALBLEIB, "Continuous-Energy Adjoint Monte Carlo Theory of Coupled Continuum/Discrete Radiation Transport," *Nucl. Sci. Eng.*, **80**, 162 (1982).

3. N. M. BORISOV and M. P. PANIN, "Adjoint Importance Monte Carlo Simulation for Gamma Ray Deep Penetration Problem," *Monte Carlo Methods Appl.*, **3**, 241 (1997).

4. T. E. BOOTH, "A Monte Carlo Variance Reduction Approach for Non-Boltzmann Tallies," *Nucl. Sci. Eng.*, **116**, 113 (1994).

5. N. M. BORISOV and M. P. PANIN, "Adjoint Monte Carlo Calculations of Pulse-Height-Spectrum," *Monte Carlo Methods Appl.*, **4**, 273 (1998).

6. D. C. IRVING, "The Adjoint Boltzmann Equation and Its Simulation by Monte Carlo," *Nucl. Eng. Des.*, **15**, 273 (1971).

7. M. KALOS, "Monte Carlo Integration of the Adjoint Gamma Ray Transport Equation," *Nucl. Sci. Eng.*, **33**, 284 (1968).

8. J. E. HOOGENBOOM, "Continuous Energy Adjoint Monte Carlo for Coupled Neutron-Photon Transport," *Proc. Monte Carlo 2000 Conf.*, Lisbon, Portugal, October 23–26, 2000, pp. 613–618.

9. J. H. HUBBEL and W. J. VEIGE, "Comparison of Theoretic and Experimental Photoeffect Data, 0.1 MeV—1.5 MeV," U.S. Department of Commerce, National Bureau of Standards, Tech. Note N 900 (1976).

10. P. V. C. HOUGH, "Low Energy Pair Production," *Phys. Rev.*, **73**, 266 (1948).

11. V. F. BARANOV, "Electron Radiation Dosimetry," *Atomizdat*, 47 (1974) (in Russian).

12. H. A. BETHE, "Molière's Theory of Multiple Scattering," *Phys. Rev.*, **89**, 1256 (1953).

13. L. KOBLINGER, "A New Energy Sampling Method for Monte Carlo Simulation of the Adjoint Transport Equation," KFKI-76-65, Budapest-76, Central Research Institute for Physics (1976).

14. J. A. WALL and E. A. BURKE, "Gamma Dose Distribution at and near the Interface of Different Matters," *IEEE Trans. Nucl. Sci.*, Vol. NS-17, *6*, 305, Institute of Electrical and Electronics Engineers (1970).

15. A. M. KOLCHUZHKIN and V. N. POTAPOV, "Calculation of Secondary Electron Fields in Inhomogenous Absorbers by Monte Carlo," in *Secondary Electron Radiation*, p. 59, V. V. SMIRNOV, Ed., V. G. Khlopin Radium Institute, Leningrad (1977) (in Russian).